Exp Astron (2013) 36:389–405
DOI 10.1007/s10686-013-9338-1

ORIGINAL ARTICLE

First results from a next-generation off-plane X-ray diffraction grating

Randall McEntaffer · Casey DeRoo · Ted Schultz · Brennan Gantner · James Tutt · Andrew Holland · Stephen O'Dell · Jessica Gaskin · Jeffrey Kolodziejczak · William W. Zhang · Kai-Wing Chan · Michael Biskach · Ryan McClelland · Dmitri Iazikov · Xinpeng Wang · Larry Koecher

Received: 22 January 2013 / Accepted: 27 March 2013 / Published online: 15 May 2013

Abstract Future NASA X-ray spectroscopy missions will require high throughput, high resolving power grating spectrometers. Off-plane reflection gratings are capable of meeting the performance requirements needed to realize the scientific goals of these missions. We have identified a novel grating fabrication method that utilizes common lithographic and microfabrication techniques to produce the high fidelity groove profile necessary to achieve this performance. Application of this process has produced an initial pre-master that exhibits a radial (variable line spacing along the groove dimension), high density (>6000 grooves/mm), laminar profile. This pre-master has been tested for diffraction efficiency at the BESSY II synchrotron light facility and diffracts up to 55 % of incident light into usable spectral orders. Furthermore, tests of spectral resolving power show that these gratings are capable of obtaining resolving powers well above 1300 ($\lambda/\Delta\lambda$) with limitations due to the test apparatus, not the gratings. Obtaining these results has provided confidence that this

R. McEntaffer (✉) · C. DeRoo · T. Schultz · B. Gantner
Department of Physics & Astronomy, University of Iowa, Van Allen Hall, Iowa City, IA 52242, USA
e-mail: randall-mcentaffer@uiowa.edu

J. Tutt · A. Holland
Centre for Electronic Imaging, The Open University, Walton Hall, Milton Keynes MK7 6AA, UK

S. O'Dell · J. Gaskin · J. Kolodziejczak
NASA Marshall Space Flight Center, 320 Sparkman Dr. NW, Huntsville, AL 35805, USA

W. W. Zhang · K.-W. Chan · M. Biskach · R. McClelland
NASA Goddard Space Flight Center, Bldg 34, Greenbelt, MD 20771, USA

D. Iazikov
LightSmyth Technologies, Inc., 875 Wilson St. Suite C, Eugene, OR 97402, USA

X. Wang · L. Koecher
Nanonex Corporation, 1 Deerpark Dr., Monmouth Jct., NJ 08852, USA

fabrication process is capable of producing off-plane reflection gratings for the next generation of X-ray observatories.

Keywords X-ray spectroscopy · Off-plane reflection gratings · X-ray diffraction

1 Introduction

Soft X-ray energies harbor a wealth of transition lines useful for performing key diagnostics in astrophysical plasmas. Grating spectrometers are employed on current X-ray observatories, such as *XMM-Newton* and the *Chandra X-ray Observatory*, and had been baselined for the recently cancelled *International X-ray Observatory* (*IXO*) program to obtain spectra in this regime. Next-generation observatories, however, will require significant improvements in spectrometer performance in order to accomplish future science goals. For example, *IXO*'s X-ray Grating Spectrometer (XGS) sought spectral resolving powers of $\lambda/\Delta\lambda > 3000$ and effective areas of $\sim$1000 cm^2 for an energy range of 0.3–1.0 keV. This represents nearly a full order of magnitude performance improvement in both specifications from the grating instruments of *Chandra* and *XMM-Newton*, thus necessitating the development of a new generation of high quality spectrometers capable of achieving these performance requirements [1].

Spectrometers employing off-plane reflection gratings are a promising approach to soft x-ray spectroscopy, offering preferable telescope packing geometries compared to an in-plane design, excellent throughput, and the potential for high resolving power in the desired bands. These spectrometers typically use a set of nested Wolter-I optics (a primary parabolic mirror, followed by a secondary hyperbolic), focusing x-rays over a length of several meters. A short distance aft of the exit aperture of the mirrors, an array of gratings positioned in the off-plane mount disperses the converging light [13]. This dispersion is in the shape of a cone (giving the common name "conical diffraction"), and forms an arc of diffracted light at the focal plane. The dispersed spectrum is then imaged by a detector, typically a CCD camera, placed at the focal plane.

The off-plane mount requires customized gratings in order to be optimized for high resolving powers and increased efficiencies. Figure 1 shows the grating geometry and illustrates how these advances can be achieved. The image on the left shows light intersecting a ruled grating nearly parallel to the groove direction creating an arc of diffraction at the focal plane with dispersion dictated by the displayed grating equation. On the right, the optical axis is out of the page and the grating grooves are shown projected from the position of the gratings all the way down to the focal plane. This distance is called the "throw" and is typically several ($\sim$7–20) meters. Obtaining high reflectivities of the X-rays necessitates grazing incidence and, in turn, arrays of aligned, stacked gratings. Such an array can obtain optimal collecting area in the off-plane mount given that the grazing angle of incoming light onto the grating is equal to the half angle of the arc of diffraction exiting the grating surface. This allows for closely spaced packing geometries that are not available to traditional in-plane reflection grating arrays, such as those on *XMM*. Furthermore, the groove surfaces can be

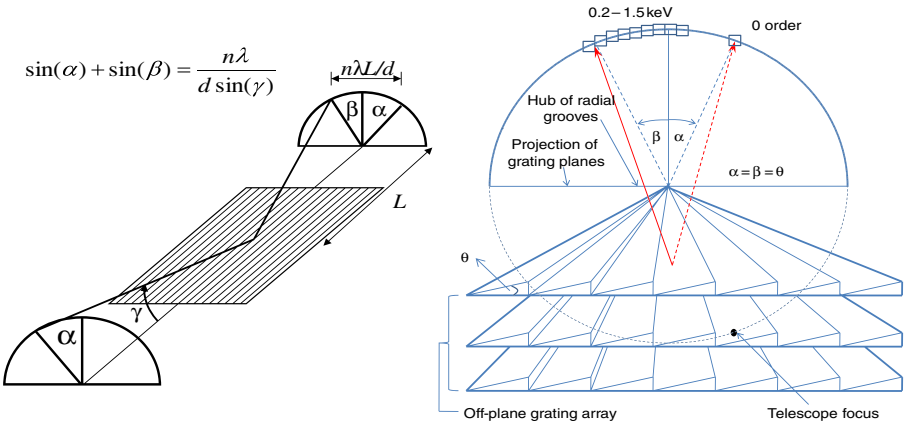

Fig. 1 *Left* - The off-plane grating mount. *Right* - Three gratings, placed many meters from the focus, are shown projected onto the focal plane to elucidate the nature of the arc of diffraction which is detected by an array of CCDs (depicted as squares)

blazed to a triangular profile that preferentially disperses light to one side of zero order. This increases the signal-to-noise for these orders and allows a smaller detector array. The blaze angle (θ in Fig. 1) is chosen to optimize diffraction efficiency at a certain wavelength, typically in the middle of the first order bandpass, which translates to optimized efficiencies at higher orders for shorter wavelengths. The grating array is then placed with the grooves at a slight angle relative to the optical axis resulting in an α for zero order at the focal plane that equals the β of the optimized wavelength. When $\alpha = \beta = \theta$ the array is optimized for diffraction efficiency.

The projection of the grooves in Fig. 1 illustrates the radial distribution of grooves necessary to achieve high spectral resolving power. The convergence of the grooves matches the convergence of the telescope beam, thus maintaining a constant α at the grating and constant β per wavelength at the focal plane, which limits groove profile induced aberration. The grooves converge to a point at the center of the circle defined by the intersection of the cone of diffraction with the focal plane. This circle also contains both the telescope focus and the zero order focus. The overlap of spectra from each of the gratings in the array is achieved by fanning the gratings such that all surfaces project to the diameter of this circle with coincident groove hubs. Another grating characteristic necessary for high spectral resolving power is high groove density. Previous mission studies, such as *IXO*, utilize telescope optics with a 5–15 arcsecond half power diameter (HPD). Off-plane grating arrays can subaperture the telescope beam [3] to create a bowtie shaped line spread function with a full width at half maximum (FWHM) of ∼1–2 arcsecond in the dispersion direction. The amount of dispersion for a grating details the physical extent over which the spectrum is diffracted and hence resolvable. Dispersion is inversely proportional to the throw and the groove density. Therefore, longer throws and/or higher groove densities can be used to spread the spectrum over a greater distance and increase spectral resolving power. A throw of several meters (> 5) and a $\sim$ 10 arcsecond telescope

HPD that can be subapertured down to ∼1–2 arcseconds translates to groove density requirements of > 5000 grooves/mm.

While the previous geometric considerations make an off-plane spectrometer an excellent candidate for future X-ray grating missions, key steps still need to be taken in the maturation of this technology. The off-plane mount requires higher groove densities in comparison to in-plane gratings and tighter alignment tolerances in comparison to transmission grating spectrometers. These issues must be addressed during the technology development roadmap. Therefore, it is our goal to develop a process for fabricating and replicating the high groove density (> 5000 grooves/mm), radially ruled, blazed gratings required for a next-generation instrument. This fabrication process must also be reproducable over large formats (∼ 100 mm ×100 mm) in order to achieve large collecting areas while maintaining the feasibility of grating alignment and mass restrictions. These four grating characteristics – radial ruling, blazed profile, high groove density, and large grating formats – represent the major technical challenges to be overcome in next-generation grating fabrication. In this paper we discuss recent advances in a novel fabrication method that is capable of overcoming these challenges in the coming years. Specifically, we discuss the fabrication and testing of a "pre-master" off-plane grating that exhibits many of the aforementioned characteristics. We present empirical results from diffraction efficiency and spectral resolving power performance tests. Finally, we discuss the path forward to increasing the fidelity of these promising gratings.

2 Off-plane grating fabrication

Holographic recording has significant heritage with previous off-plane reflection grating studies [11, 12, 15, 16]. These gratings have been employed in multiple suborbital rocket flights and were explored during the *IXO* development effort. This method of fabrication involves the interference of two recording laser beams onto a photoresist coated substrate. The light sources are placed within the plane containing the grating normal and perpendicular to the eventual groove direction. This method has created parallel grooves at moderate to high densities (4500–5670 gr/mm). Subsequent etching techniques can be used to blaze the grooves while out-of-plane displacements of the recording sources can produce pseudo-radial groove profiles. However, several limitations currently exist with this technology: higher groove densities require smaller wavelength lasers; reliable recording over large scales has not been accomplished and requires new tooling; and the radial profile is an approximation that results in a non-zero grating induced aberration. These issues could likely be resolved with significant upgrades to production facilities. However, uncertainty in the future of the technology development of off-plane grating technology can be removed by identifying suitable fabrication alternatives that take advantage of current, common techniques.

We have begun to explore a novel grating fabrication method that integrates three common microfabrication techniques: e-beam writing of a photomask, deep ultraviolet (DUV) projection lithography, and anisotropic etching. Gratings produced with this integrated method can possess a high groove density with a blazed, radial

profile and can be replicated over large formats, hence meeting the requirements for a new generation of off-plane reflection gratings. The first two steps in this process produce a "pre-master" exhibiting a high-density, laminar, radial groove profile. Fabrication of the pre-master using e-beam writing and DUV projection lithography is a technique developed by LightSmyth Technologies. This method employs computer aided design (CAD) to define the width and location of each grating groove resulting in a series of polygons. The design is done at four times the scale of the actual grating layout. The CAD design programs an e-beam writing tool to create a photomask with a very fine mesh spacing of 1 nm, much smaller than the grooves but relevant for the radial geometry patterning. The input design for the DUV mask uses a perfect radial profile with each groove angularly offset with respect to the next groove by ∼4 milliarcsec. While writing the mask, the tool snaps to the closest grid in the 1 nm mesh defining the tool resolution. The mask is prepared from an ultra-flat fused silica plate coated with a film of chromium overcoated with a layer of photoresist. The resist is exposed in the e-beam writer in accordance with the CAD file pattern, then developed to remove the exposed portions. The groove pattern is transferred into the chromium film using a reactive ion etch (RIE). The resulting mask exhibits strips of chromium corresponding to the locations of the grooves and transparent areas in the location of the grating trenches.

The mask pattern is subsequently reduced onto a resist coated, single crystal Si wafer via 4x reduction projection lithography. The DUV projection step is performed using immersion lithography with 193 nm light to pattern a photoresist coated Si wafer. This effectively reduces the step size to 0.25 nm to create the closest approximation to the radial profile currently achievable. The result can be effectively thought of as 3 sections along the 32 mm direction ranging from 6024–6042 grooves/mm (165.5–166 nm periods). The step-like transitions between these sections is blurred somewhat during the DUV step, thus increasing the fidelity of the radial approximation. After the resist has been developed the exposed resist is chemically removed. Next, a reactive ion etch (RIE) is used to transfer the pattern into the Si wafer before the remaining resist is removed by a chemical wash. Finally, gold film was deposited on the silicon grating using an e-beam coating chamber in a top-down deposition geometry. The chamber was specially designed by LightSmyth to ensure high fidelity of the gold grating that accurately reproduces the surface corrugation on the Si wafer after ∼80 nm of gold deposition.

These densities obtained by the pre-master fabrication process are very high and easily achieve the dispersion required for a next-generation off-plane grating. In addition, the recorded radial profile is the best to date thus achieving two of our goals. The limitation is that the final product is not blazed but a laminar groove profile. However, common, straightforward, post-processing techniques can sculpt the grooves to achieve the desired blazed profile. Anisotropic etching is capable of producing gratings with atomically smooth, blazed groove facets but has currently not been used to make a radially fanned groove distribution. A process to manufacture blazed gratings of moderate groove density (5000 gr/mm) using anisotropic etching was developed at MIT [4], and exploits a preferred direction for KOH etching in single crystal Si. We are currently exploring a similar process which is summarized in Fig. 2. By combining laser recording with an anisotropic etching process, it would be possible to

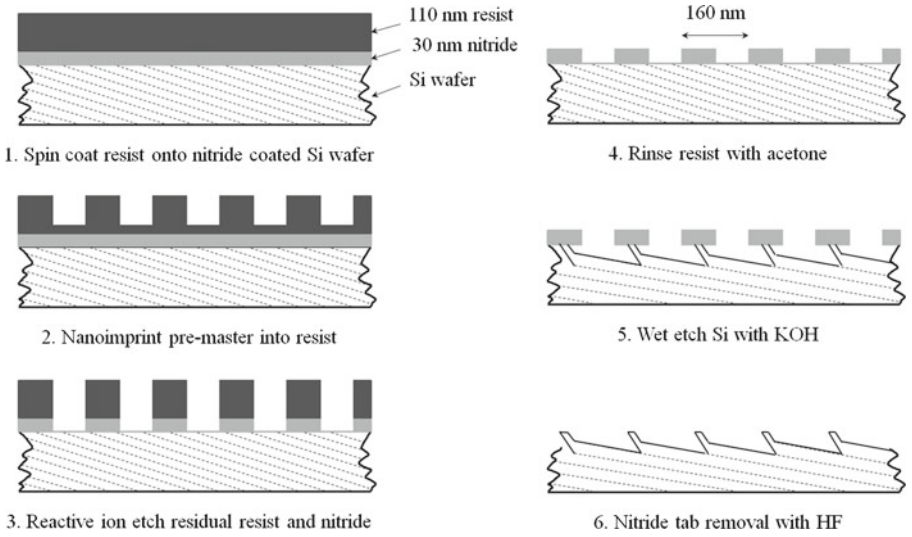

Fig. 2 Fabrication methodology for blazed, off-plane reflection gratings on Si wafers

exploit the high fidelity radial profile produced by LightSmyth while obtaining a high quality blaze.

The novel aspect of our procedure is the use of nanoimprint lithography to transfer the pre-master pattern into a nanoimprint resist [5, 7]. The pre-master is used as a patterned mold that is pressed into the resist to transfer the pattern, similar to embossing. This technique can be used to reproduce features on the nanometer scale [6] and can also be applied over large formats (up to 8 inch wafers). Once the pre-master has been imprinted into a resist coated wafer, an RIE run transfers the pattern into the nitride coating. Residual resist can be rinsed off with acetone leaving the groove pattern in nitride strips on the Si wafer. The wafer can be cut off-axis so that the (111) crystallographic plane of Si is at an angle relative to the plane of the wafer. This angle represents the blaze angle of the grooves. A KOH etch preferentially etches along the (111) plane leaving atomically smooth, and hence scatter limited, angled facets between the nitride tabs, which are subsequently removed with HF. The effect of the nitride tabs can be removed with a subsequent nanoimprint replication step [4] or etched away. A reflective coating is then applied to the surface resulting in a blazed, radially ruled, high density grating with excellent X-ray reflectivity at grazing incidence. All of the above processes can be applied to large formats as well, thus making them applicable to future generations of off-plane gratings.

3 Pre-master characterization

The first step in investigating this integrated process is the fabrication and characterization of the high quality pre-master. To that end, LightSmyth has produced a series of high groove density, laminar gratings over a 25×32 mm format with grooves along

the 32 mm direction. The groove distribution for these gratings is radially ruled to match the convergence of an 8.4 m telescope beam - the focal length of the test optics used during spectral resolving power performance testing. Figure 3 shows scanning electron microscope (SEM) images of these gratings. The cross-section image on the left displays an exceptionally clean groove profile with a feature size of ∼84 nm, period of ∼163 nm, and etch depth of ∼60 nm in single crystal Si. The excellent profile is maintained even after the reflective Au coating has been applied as shown in the image on the right of this figure. This image shows the same Si profile from the left image as the black substrate on the bottom half of the picture. The Au coating appears gray and the profile is slightly rounded off at the corners of the groove features causing them to appear more trapezoidal than rectangular.

3.1 Diffraction efficiency

Establishing that the pre-master has clean, non-distorted groove profiles and low surface roughness is essential, as any aberrations will be transferred during the subsequent replication process. While the SEM images are strong evidence that the pre-master meets these criteria, performance testing of the pre-master is necessary to provide crucial insight into the processing steps of these gratings. Testing will provide assurance that the initial steps of the process are at a high enough fidelity to produce the quality of grating expected further down the fabrication chain. As such, a testing campaign to measure the diffraction efficiency of the grating was conducted at the Physikalisch-Technische Bundesanstalt (PTB) soft X-ray beamline located at the BESSY II synchrotron [10, 17]. This facility utilizes a grating monochromator sampling the electron storage ring to create a 98 % polarized beam with tunable X-ray energies from ∼0.1–1.9 keV. The test chamber houses staging allowing for sample alignment with six degrees of freedom. Most importantly for the off-plane configuration, the detector photodiode can scan in two dimensions to sample the entire focal plane.

The grating was tested from 0.3–1.5 keV with 50 eV steps for three graze angles. Figure 4 demonstrates the testing methodology showing a raytrace of zeroth order

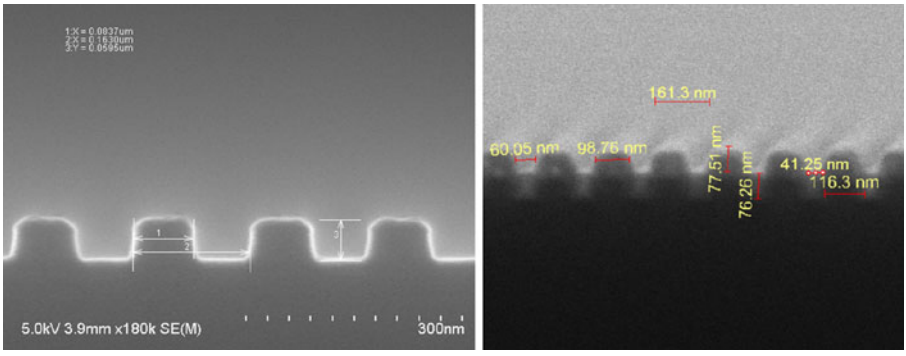

Fig. 3 *Left* - Cross-section SEM image of the laminar groove profile on single crystal Si. *Right* - The same Si profile is seen in black with a gray e-beam deposited Au layer on top

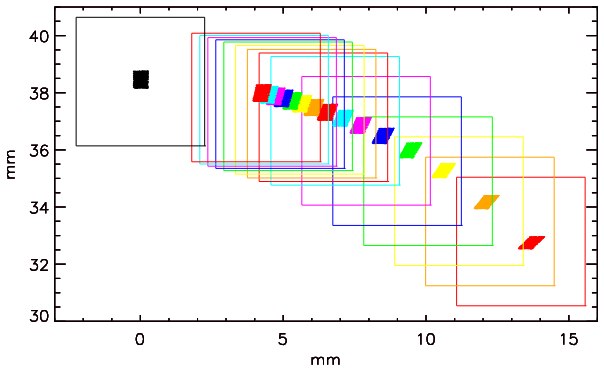

Fig. 4 The raytrace of the expected arc of diffraction is shown as a series of 16 small scatter plot rectangles with zero order in black and the 15 tested energies from 0.3–1.0 keV in a rainbow of colors. Associated diode positions for each energy are shown as larger squares with the corresponding color

and the arc of diffraction expected from the 15 energies tested at an incidence angle of 88° (graze angle of 2°). We show the position of the diffracted spots as derived via raytrace, with each spot measuring 0.5 mm horizontally and 0.6 mm vertically (the grating plane is horizontal), which is the typical beam aperture at the position of the test sample. The direct beam is located at the origin and the throw is $\sim$ 550 mm. We overlay squares representing the larger diode area, 4.5 $\times$ 4.5 mm. The positions used for these diode positions are derived from those actually used during testing to show the congruence between the raytrace expectations and the empirical test setup. At each energy the photodiode only samples a single order, even at the highest energies. The raytraced spots display an aberration that skews the aperture rectangle into a parallelogram. This affect is caused by the finite size of the beam on the grating leading to path length differences at the focal plane when considering one horizontal limit of the beam versus the other. It is more noticeable at long wavelengths where dispersion is highest leading to the largest path length differences. However, given that the size of the diode is much larger than the aperture, the aberration does not effect the efficiency measurements.

Figure 5 displays the measured diffraction efficiencies for the BESSY campaign. The direct beam current at the photodiode is measured to serve as the reference for the incident flux. The grating is then placed in the beam and the photodiode is moved in two dimensions to scan the arc of diffraction and measure the diffracted flux. The absolute efficiency is the ratio of these fluxes, and therefore includes the effect of the Au reflectivity. The incident fluxes are normalized using measurements of the synchrotron ring current. The uncertainty in the measurement is dominated by the stability of the beam current which decays over time for a synchrotron light source. Over the time scale of an energy scan we measured a maximum current decay of 6 % with 2–3 % typical. The 6 % uncertainty is indeed a worse case scenario, and in practice is much less given the linear decay of the current, yet can be used as an upper limit to the flux measurement error, which results in a $\sim$ 3 % absolute efficiency error. Results are shown for graze angles of 2° (top row), 1.5° (middle row), and 1°

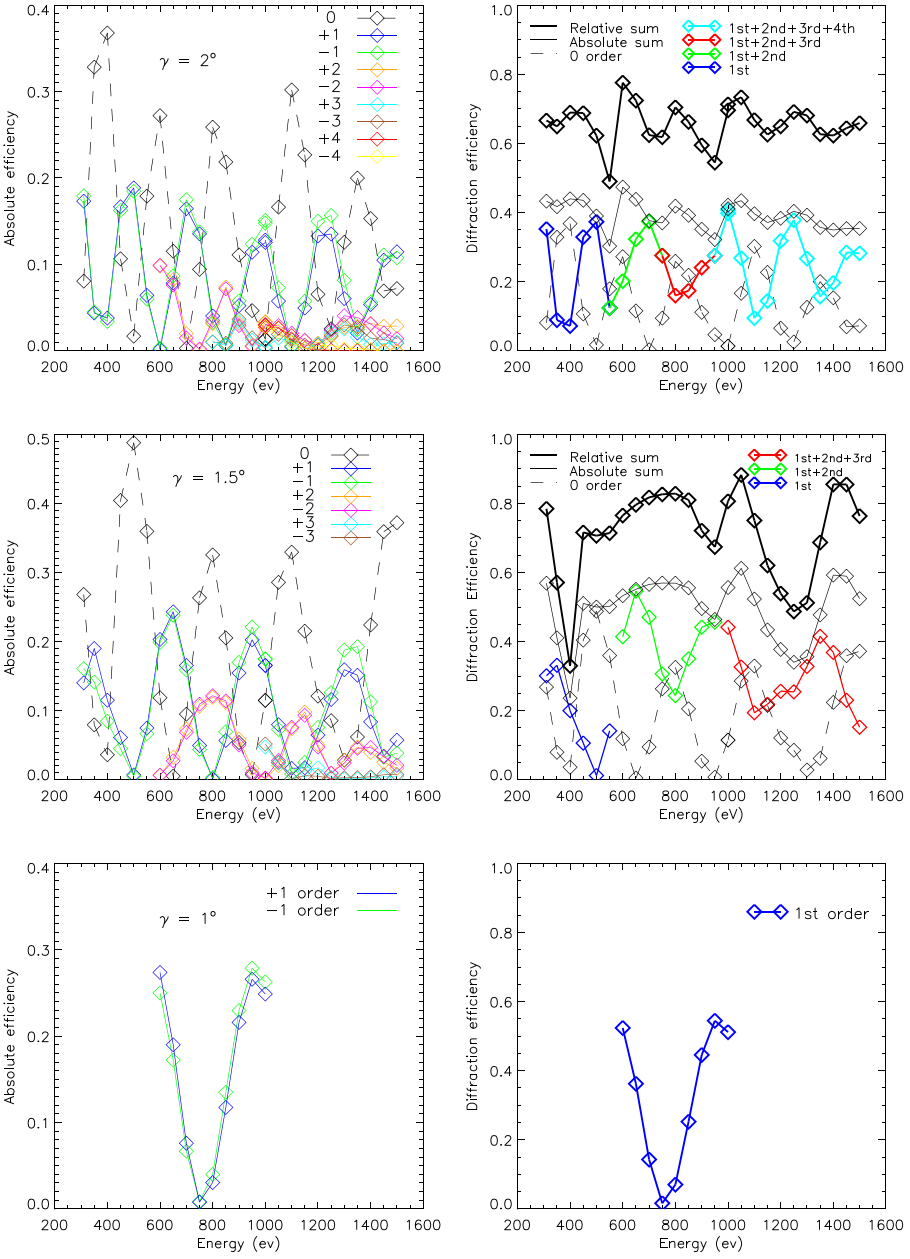

Fig. 5 Measured diffraction efficiencies at graze angles of 2° (top row), 1.5° (*middle row*), and 1° (*bottom row*). Measurements of individual orders are shown in the left column as absolute efficiencies which include the reflectivity of Au. Summed order efficiencies are shown in the right column. The thin, solid black line shows the total absolute efficiency of all orders, including zero order; the thick, solid black line shows the total relative efficiency which factors out the effect of the Au reflectivity

(bottom row). The left side of the figure gives absolute efficiencies at each measured order; the right side shows overall diffraction efficiencies through summation of orders. It is important to note that the grating was tested at $\alpha = 0$ (light parallel to the grooves). This led to a limitation on available orders at low energy, which results in only one or two measurable orders over a significant range of our bandpass for this configuration. The effect of the laminar profile is evident: There are large contributions to zero order, the positive/negative orders contain a nearly equal number of photons, and the diffraction pattern is quite regular and stable over a large range of energies. This symmetry of positive/negative orders is important, as it indicates minimal asymmetry in the groove profile across the grating, which will result in a cleaner groove profile being transferred into the resist during the subsequent nanoimprint process. Furthermore, there is a noticeable periodicity in the efficiency as a function of energy which is driven by interference between wavefronts originating from the groove trenches and the flat tops of the grooves. This interference pattern is removed once the grooves are blazed resulting in one broad hump and a more continuous response with energy.

At 2°, the sum of diffracted orders range from 10–40 % in absolute efficiency with 30–40 % being typical. When considering zero order contributions, the total amount of light in the arc of diffraction averages around 70 % after dividing by the Au reflectivity [8]. At the 1.5° graze angle the relative efficiency averages $>$ 10 % more total light into the arc of diffraction than that observed at 2° after removing the dependence of the Au reflection efficiency. At 1.5° the absolute efficiency of diffracted orders is consistently above 40 % when multiple orders are present and greater than 50 % at 650 eV. Of the few energies we were able to measure at a 1° graze angle, we again find efficiencies that are well above 50 % at 600 eV and from 950–1050 eV. Given the small graze angle and the $\alpha = 0$ configuration, only $\pm$1st order are available (zero order was present but not measured). Overall, the gratings consistently produce efficiencies above 30 % and up to 55 %.

While at BESSY, in addition to efficiency testing, the diffracted beam was also directed onto a CCD camera to image the arc of diffraction. Given the small number of access ports on the PTB test chamber, the camera was placed along the beam axis thus limiting the graze angle to 0.25° and our spectral range to only the highest energies. Even so, we were able to run the monochromator at 1.9 keV and image two diffraction orders along with zero order on a single CCD. In this configuration, the throw is 2.8 m and the grating is rotated 0.23° about its normal to provide an appropriate α to accommodate multiple orders. As shown in Fig. 6, the diffraction properties of the grating match the theoretical raytrace, providing further verification on the high quality of the groove profile. In the raytrace the entire beam is traced when in actuality the grating only samples a thin section at this low graze angle resulting in an aperture that no longer appears rectangular, but more diffuse. However, the placement of orders and the rotation of the image as a function of order are observed. Close inspection of these data show no obvious sign of scatter off of the grating surface which should be preferentially in the in-plane or vertical direction [11]. The reflection direction is up which is also where the sharp edge of the image appears. In the case of significant scatter, the sharp edge will become diffuse and extended

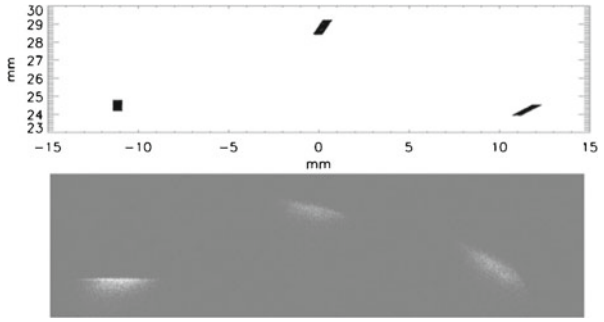

Fig. 6 The upper plot is a raytrace of the pre-master in the BESSY beamline onto the CCD focal plane. The spot on the left is the zero order image of the slit using 1.9 keV with 1st and 2nd order diffracted toward the right. The lower plot is a CCD image of the actual arc of diffraction for 1.9 keV X-rays, and agrees with the raytrace predictions. The physical horizontal size of the CCD is 26 mm

upward, along the plane of incidence. This effect is not seen in these data. However, due to time limitations we were not able to properly count photons with the CCD to determine the fraction of flux detectable as scatter, and hence, perform a quantitative assessment.

3.2 Spectral resolving power

In addition to diffraction efficiency, the science goals of future observatories require high spectral resolving power for the next generation of gratings. For the *IXO* project this translated to requiring $\lambda/\Delta\lambda > 3000$ over a 0.3–1.0 keV band. This energy range is limited on the low end by the response of the CCD camera. The high end will be determined by comparing the resolutions and sensitivities between gratings and microcalorimeters, but will most likely lie between 1.0–2.0 keV. The major hurdle to obtaining high spectral resolving power in the off-plane mount is producing a high fidelity radial groove profile. As explained in Section 2, the pre-masters approximate this profile by using several parallel sections with groove density increasing in the direction toward the focal plane. The pre-master was tested for spectral resolving power at NASA's Marshall Space Flight Center (MSFC) Stray Light Facility (SLF). This is a 100 m beamline utilizing a Manson electron impact X-ray source at one end with a large 3 m diameter, 10 m long instrument chamber at the opposite end to house the experiment. We utilized a Wolter-I telescope fabricated at NASA's Goddard Space Flight Center (GSFC) to create the focused beam [18]. Glass slumping onto precision mandrels is used to create the parabola/hyperbola pairs. We used a Technology Development Module (TDM) that has three pairs of these mirrors aligned to create a <10 arcsecond HPD focus at a nominal focal length of 8.4 m. These mirrors only cover $\sim 30°$ of azimuth thus resulting in a subapertured beam with a much tighter focus in one dimension. We subapertured the beam even further given that our gratings are only 25 mm wide ($\sim 6°$ of azimuth). The mirror focal length at the finite conjugate (90 m source distance) is ~ 9.3 m.

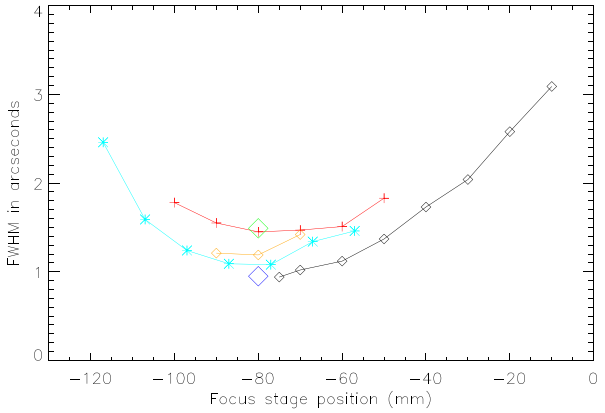

Fig. 7 Zero order focus results: Black diamonds - focus run on Day 1 with Manson electron beam current at 0.16 mA; Red crosses - focus run on Day 2 with Manson beam current at 0.5 mA; Cyan asterisks - focus run on Day 3 with Manson beam current at 0.16 mA; Green and Blue diamonds - focus checks on Day 4 with Manson beam at 0.5 mA and 0.16 mA, respectively; Orange diamonds - focus check on Day 5 with Manson beam at 0.16 mA

The test began with finding a focus for zero order. Focus runs were performed each day and the results are summarized in Fig. 7. The best focus obtained in the dispersion direction was 0.94 arcseconds full width at half maximum (FWHM) on Day 1. Even though the quality of the focus varied slightly day-to-day, a much larger effect was observed by changing the electron beam flux at the Manson source. The impact source utilizes a high potential field (several kV) to accelerate electrons into a solid anode, in this case Mg, to create fluorescence lines. Such resolving power tests are often flux limited so it is typically a necessity to maximize the source flux. This is done through increasing the electron beam current of the Manson, or in other words the number of electrons allowed to impact the anode. As the stream of electrons increases, so does the repulsive Coulomb force in the beam causing the size of the impact spot to increase as well. Therefore, at high flux one typically observes a larger impact spot on the anode. We found that the GSFC TDM is capable of resolving the impact spot at 90 m (1 arcsecond ∼0.44 mm) even at the lowest beam current setting (0.16 mA), resulting in a diffuse source. This applies a systematic limit to the spectral resolving power that is necessarily factored into the results.

On Day 2 we performed repeated measurements of the first order lines. In general, these measurements were made at high beam current, given that we were concentrating on imaging and alignment. Post alignment, we turned down the beam current and obtained our best first order resolution. An image and histogram of the line are given in Fig. 8. We measured the diffraction distance between zero order and first order and the width of the line to obtain spectral resolving power. We assume that the horizontal dimension is aligned with the dispersion direction. While we took care in leveling all test equipment, it is possible that these dimensions are not perfectly aligned, thus adding systematic error. In the absence of misalignment, the distance between zero order and first order was measured to be 50.96 ± 0.03 mm. The error is dominated

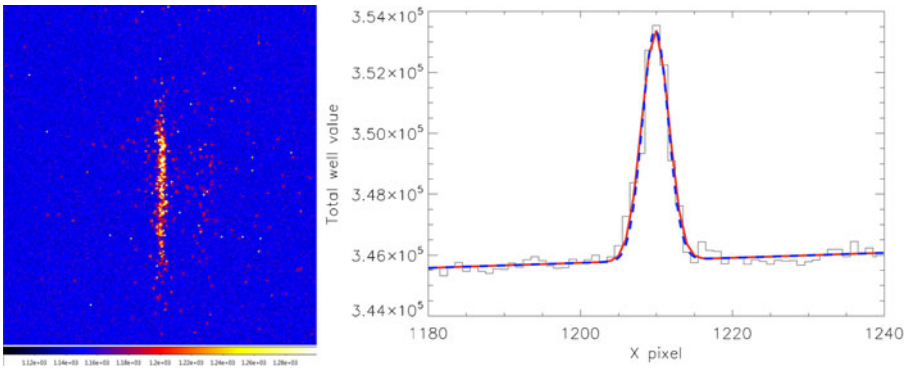

Fig. 8 *Left*–CCD image of the first order Mg Kα line. *Right*–Histogram of all CCD counts with best fit overlaid in red and theoretical expectation in dashed blue

by the uncertainty in the Gaussian fits to the lines as opposed to measurement uncertainty in the CCD linear stages. The Gaussian fit to first order (red curve in Fig. 8 has a FWHM of 4.2 ± 0.1 pixels, or 0.057 ± 0.001 mm, given 13.5 μm pixels. This gives a spectral resolving power of $x/\Delta x = 894 \pm 16$. For verification, this number can be used to back out the groove density. Using $\lambda/\Delta\lambda = 894$ at Mg Kα (9.89 Å) yields $\Delta\lambda = 0.0111 \pm 0.0002$ Å. The grating dispersion can then be written as $\Delta\lambda/\Delta x = 10^7/(\text{groove density} \times \text{throw}) = 0.19$ Å/mm. Given the measured throw of 8.52 ± 0.01 m, the resulting groove density is 6100 ± 150 grooves/mm, consistent with expectations.

Also shown in Fig. 8 is the theoretical expectation of the first order line, represented by the dashed blue line. The theoretical resolving power must factor in the line spread function of zero order, the expected aberration from the radial groove approximation, and the natural width of the line. The aberration caused by the radial groove approximation has been raytraced using Interactive Ray Trace (IRT; v2.7). The raytrace calculates a grating contribution of 0.47 arcseconds (FWHM) to the spectral line spread function. Therefore, given a point source and a scatter dominated telescope focus, this grating is capable of achieving theoretical first order resolving powers above 2500. However, the source is resolvable and the telescope has figure errors that contribute to the telescope HPD such that the zero order focus at the time of first order testing was 1.1 arcseconds. Summing these errors results in a 1.2 arcsecond FWHM which as seen in Fig. 8 characterizes what we measured quite well. Even so, theory suggests a slightly tighter FWHM than that measured. This small difference does yield a slightly higher theoretical resolving power of 996, but practically is only 1/5 of a pixel. There may be several factors that are contributing to this small difference: an assumption that the lines are perfectly vertical on the CCD, split events contributing to the width, fluctuating Manson flux levels, unstable mirror focus with temperature, a small deviation in the optical focal plane, etc. Furthermore, the natural width of Mg Kα has been calculated as 0.36 eV, giving theoretical resolutions of $\sim$ 3500 ($E/\Delta E$), which should not effect the line spread function [9]. However, empirical measurements show that a more reasonable line width may be

0.0035 Å[2], which would reduce the theoretical value to a resolving power of 939, less than 3σ from the measured value. Given these factors the measured resolving power is remarkably close and likely consistent to the theoretical limit.

Second order testing occurred on Day 5 when the best zero order focus obtained was 1.19 arcseconds at low beam current. Sampling of the focal plane was limited by the maximum displacements of the linear stages controlling the CCD position. Therefore, to image higher order spectral lines we had to apply an α to the grating to position the arc of diffraction at a vertical and horizontal position consistent with the linear stage ranges. This necessitated a larger graze angle as well and ultimately resulted in much lower efficiency in the second order line. We therefore operated at high Manson flux, 0.4 mA, resulting in an intrinsically larger spot. Given the low number of counts at the focal plane, we operated in photon counting mode which takes 270 individual 30 second exposures over 3.5 hours. When analyzing this data cube we only consider counts that are 5σ above the median value of an individual 30 second exposure, where σ is the standard deviation pixel value in the individual image. The charge in the surrounding 8 pixels is summed for each pixel above this 5σ threshold. This results in a total photon count of 93 photons. The resulting line and histogram of counts are shown in Fig. 9. While this number is lower than optimal, it represents only those counts that are well above the background. The photon counts can be significantly increased with lower CCD backgrounds (typical background pixel ~90 counts; typical photon pixel ~150 counts with splits decreasing significance per pixel) and more optimal grating configurations. The width of the 2nd order line is 5.48 pixels resulting in a 1.64 arcsecond focus. Given the grating dispersion this results in a resolving power of 1375. Again, this matches well with the observed $x/\Delta x$ dispersion of 98 mm/0.074 mm = 1324. It is expected that a second order line

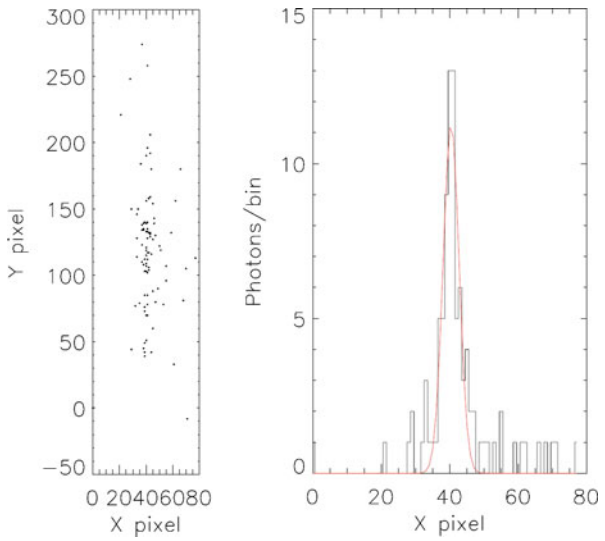

Fig. 9 *Left*–Second order line reconstructed from only $> 5\sigma$ events. *Right*–Histogram of these photons with best fit Gaussian overlaid in red

will achieve a resolving power 2× that of 1st order, i.e. ∼1800. Instead, the measured 2nd order line width is 1.64 arcseconds, but this may be expected given our operation at 0.4 mA of beam current. We did not measure the focus at this source level, but did see 1.2 arcseconds at 0.16 mA earlier in the day and 1.5 arcseconds at 0.5 mA the day before. Using the latter convolved with the expected grating induced aberration results in a 1.6 arcsecond beam. Therefore, we once again found the resolving power to be limited by the source size. Furthermore, the 2nd order data were taken just after the chamber vacuum was interrupted by a cryo pump self-shutdown resulting from a lack of liquid nitrogen. Significant temperature deltas were observed on this day, possibly resulting in poorer telescope resolution on top of the finite source size.

4 Summary and future work

In the context of future NASA X-ray missions, X-ray grating spectrometers must be able to achieve high throughput and high spectral resolving power. Our goal is to realize this performance by utilizing off-plane reflection gratings. We have identified a novel grating fabrication technique that is capable of producing the radial, blazed, high density profile that is required to obtain this goal. The unique first step involves creating a pre-master laminar grating in single crystal Si through e-beam production of a mask with subsequent DUV lithography. This step has been accomplished and has created a radial profile grating matching an 8.4 m focal length beam with very high groove density, 6033 grooves/mm. This pattern will be transferred via nanoimprint lithography to a resist coated master that will undergo subsequent etching steps to ultimately create the blazed groove profile. These latter steps have been performed by others and are well understood leaving just the qualification of the pre-master as an open issue. We have performed this qualification and have found that the pre-master performance is consistent with our goal throughput and resolving power numbers. The non-blazed, laminar profile consistently diffracts > 30 % of incident light into usable spectral orders and upwards of 55 % in some cases. When multiple orders are present the sum of orders is typically > 40 %. Blazing this profile should produce a consistent 40 % diffraction efficiency. Furthermore, we have obtained theoretical spectral resolving powers using a high-quality X-ray optic. We found resolving powers of ∼900 in first order and >1300 in second order. These values are limited by the finite source size used in the experiment with much higher resolving powers theoretically and practically possible.

Due to a lack of time at the synchrotron facility, we were not able to perform the efficiency tests at α angles other than zero. At higher α we would be able to probe higher order diffraction at lower energies. However, large α angles are not optimal given the existing laminar profile which leads to significant groove shadowing and large diffraction angles off of steep side walls. This underscores the necessity of the blazing process. Blazed grooves will allow for maximal illumination of the grooves at a constant angle ($\alpha = \theta$) resulting in the ability to test at high α. At large α the zero order image is closer to the plane of the grating (see Fig. 1). Therefore, not only is dispersion preferentially on one side of zero order, it disperses to larger β and higher orders as well. Ultimately this results in minimal zero order contribution,

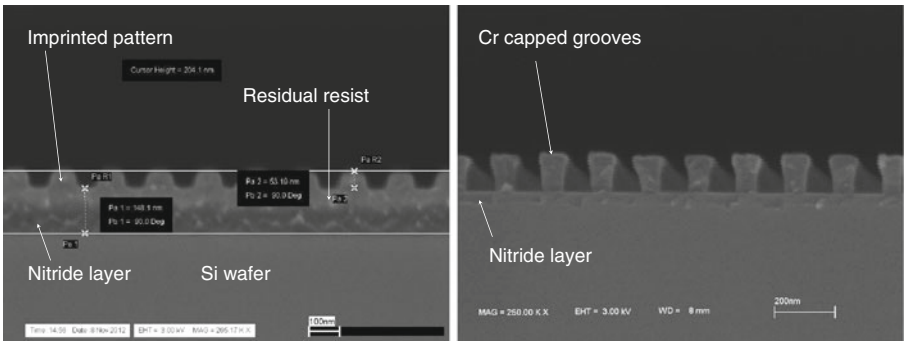

Fig. 10 *Left*–SEM image of the imprinted pattern in the resist of the secondary wafer. *Right*–The same wafer after removal of the residual resist via oxygen RIE

and additional contributions from higher orders. In such a configuration we lose the periodicity as a function of energy caused by groove trough/top interference, and the sum of diffracted orders resembles the solid black lines on the right side of Fig. 5. The effect of a dominant diffraction contribution is already seen over small energy ranges: around 1000 and 1250 eV at 2°; around 850, 950, and 1350 eV at 1.5°. At these higher energies there are typically multiple diffraction orders with minimal contributions from zero order, thus approximating what we would see more ubiquitously given blazed facets on these gratings.

The 40 % absolute efficiency limit is an important goal. Previous studies pointed toward the possibility of achieving this level for the off-plane configuration [11]. Using these initial tests, conceptual designs for instruments onboard future NASA missions – such as the *Warm-Hot Intergalactic Medium Explorer* (*WHIMEx*) and *IXO* XGS [1, 14] – have assumed 40 % diffraction efficiency as the basis for determining spectrometer properties. The assumption of obtaining this efficiency level flows down to the size of the array, the number of gratings, their size/mass/material, etc. In short, the design of the grating assembly depends heavily on their efficiency. These comprehensive BESSY tests show that the efficiencies assumed in previous IXO designs are obtainable, even with an unoptimized pre-master.

The next step will be to test the performance of blazed, radial gratings. The first step in creating this grating, nanoimprint lithography, has been accomplished by our industrial partners at Nanonex using our pre-masters as shown in Fig. 10. The SEM image on the left shows the pre-master pattern imprinted into a thick resist layer on a nitride coated Si wafer. The residual resist is removed by masking the tips of the grooves with a Cr shadow coat and oxygen plasma etching via RIE. Etching of the nitride and a wet etch of the Si will create the necessary blazed profile. Once the blazed profile has been obtained we will calculate theoretical diffraction efficiencies using PCGrate software to compare to empirical results. We will also perform measurements to quantify the amount of scatter from these etched gratings. Performance testing for throughput and resolving power on these samples will verify this process as a leading tool in next generation diffraction grating fabrication.

Acknowledgments This work was supported by NASA grants NNX12AF23G and NNX12AI16G. We would also like to acknowledge internal funding from the University of Iowa in support of Casey DeRoo. Special thanks are due to several people including Christian Laubis and his terrific support crew at PTB as well as James Carter and Bill Jones at MSFC for support of the resolution tests.

References

1. Bautz, M.W., et al.: Concepts for high-performance soft X-ray grating spectroscopy in a moderate-scale mission. Proc. SPIE **8443**, 15–23 (2012)
2. Canizares, C.R., Davis, J.E., Dewey, D., Flanagan, K.A., Galton, E.B., Huenemoerder, D.P., Ishibashi, K., Markert, T.H., Marshall, H.L., McGuirk, M., Schattenburg, M.L., Schulz, N.S., Smith, H.I., Wise, M.: The chandra high-energy transmission grating: design, fabrication, ground calibration, and 5 years in flight. Publ. Astron. Soc. Pac. **177**, 1144–1171 (2005)
3. Cash, W.: X-ray optics: a technique for high resolution imaging. Appl. Opt. **26**, 2915–2920 (1987)
4. Chang, C.-H., Heilmann, R.K., Fleming, R.C., Carter, J., Murphy, E., Schattenburg, M.L., Bailey, T.C., Ekerdt, J.G., Frankel, R.D., Voisin, R.: Fabrication of sawtooth diffraction gratings using nanoimprint lithography. J. Vac. Sci. Technol. B **21**(6), 2755–2759 (2003)
5. Chou, S.Y., Krauss, P.R., Renstrom, P.J.: Imprint lithography with 25-Nanometer resolution. Science **272**, 85 (1996)
6. Chou, S.Y., Krauss, P.R., Zhang, W., Guo, L., Zhuang, L.: Sub-10 nm imprint lithography and applications. J. Vac. Sci. Technol. B **15**(6), 2897–2904 (1997)
7. Gao, H., Tan, H., Zhang, W., Morton, K., Chou, S.Y.: Air cushion press for nanoimprint across a 100 mm field. NanoLett. **6**(11), 2438–2441 (2006)
8. Henke, B.L., Gullikson, E.M., Davis, J.C.: X-ray interactions: photoabsorption, scattering, transmission, and reflection at $E = 50 - 30000$ eV, $Z = 1 - 92$. At. Data Nucl. Data Tables **54**(2), 181–342 (1993)
9. Krause, M.O., Oliver, J.H.: Natural widths of atomic K and L levels, Kα X-ray lines and several KLL auger lines. J. Phys. Chem. Ref. Data **8**, 329–338 (1979)
10. Laubis, C., Scholze, F., Ulm, G.: Metrology in the soft X-ray range - from EUV to the water window. Proc. SPIE **7101**, 1U1–12 (2008)
11. McEntaffer, R.L., Osterman, S.N., Cash, W., Gilchrist, J., Flamand, J., Touzet, B., Bonnemason, F., Brach, C.: X-ray performance of gratings in the extreme off-plane mount. Proc. SPIE **5168**, 492–504 (2004)
12. McEntaffer, R.L., Cash, W.: Soft X-ray spectroscopy of the cygnus loop supernova remnant. Astrophys. J. **680**, 328–335 (2008)
13. McEntaffer, R.L., et al.: Developments of the off-plane x-ray grating spectrometer for IXO. Proc. SPIE **7732**, 48–60 (2010)
14. McEntaffer, R.L., Cash, W., Lillie, C., Casement, S., Zhang, W., Holland, A., Murray, N., O'Dell, S., Schattenburg, M., Heilmann, R., Tsunemi, H.: Development of off-plane gratings for WHIMex and IXO. Proc. SPIE **8147**, 81471K–81471K–11 (2011)
15. Oakley, P.H.H., McEntaffer, R.L., Cash, W.: A suborbital payload for soft X-ray spectroscopy of extended sources. Exp. Astron. **31**, 23–44 (2011)
16. Osterman, S.N., McEntaffer, R.L., Cash, W., Shipley, A.: Off-plane grating performance for Constellation-X. Proc. SPIE **5488**, 302–314 (2004)
17. Tummler, J., Brandt, G., Eden, J., Scherr, H., Scholze, F., Ulm, G.: Characterization of the PTB EUV reflectometry facility for large EUVL optical components. Proc. SPIE **5037**, 265–273 (2003)
18. Zhang, W.W., et al.: Next generation astronomical x-ray optics: high angular resolution, light weight, and low production cost. Proc. SPIE **8443**, 0S1–9 (2012)